Bulletin of the Seismological Society of America, Vol. 86, No. 4, pp. 972–980, August 1996

Earthquake Mechanisms from Linear-Programming Inversion of Seismic-Wave Amplitude Ratios

by Bruce R. Julian and G. R. Foulger

Abstract The amplitudes of radiated seismic waves contain far more information about earthquake source mechanisms than do first-motion polarities, but amplitudes are severely distorted by the effects of heterogeneity in the Earth. This distortion can be reduced greatly by using the ratios of amplitudes of appropriately chosen seismic phases, rather than simple amplitudes, but existing methods for inverting amplitude ratios are severely nonlinear and require computationally intensive searching methods to ensure that solutions are globally optimal. Searching methods are particularly costly if general (moment tensor) mechanisms are allowed. Efficient linear-programming methods, which do not suffer from these problems, have previously been applied to inverting polarities and wave amplitudes. We extend these methods to amplitude ratios, in which formulation on inequality constraint for an amplitude ratio takes the same mathematical form as a polarity observation. Three-component digital data for an earthquake at the Hengill-Grensdalur geothermal area in southwestern Iceland illustrate the power of the method. Polarities of *P*, *SH*, and *SV* waves, unusually well distributed on the focal sphere, cannot distinguish between diverse mechanisms, including a double couple. Amplitude ratios, on the other hand, clearly rule out the double-couple solution and require a large explosive isotropic component.

Introduction

It is common practice to determine earthquake mechanisms from the polarities of the first motions of *P* phases. Polarity data alone often provide adequate resolution if mechanisms are constrained to be double couples (fault-plane solutions), but it is now clear that such a constraint is not always justified. Some earthquakes, especially in volcanic and geothermal areas, have non-double-couple mechanisms that require the more general moment-tensor representation (Foulger, 1988; Julian *et al.,* 1996a; Miller *et al.,* 1996).

Resolving general moment-tensor earthquake mechanisms using polarity data alone is surprisingly difficult. Even when seismometers are distributed well, there usually exist a wide range of mechanisms that are consistent with observed polarities. To overcome this difficulty, it is necessary to supplement first motions, for example, with amplitude data. The use of amplitudes is hindered, however, by our ignorance about the structure of the Earth. Focusing and defocusing effects distort observed amplitudes in a way that is extremely sensitive to structural details. Realistic three-dimensional Earth models are seldom available, and accurately computing seismic-wave propagation in them is not yet feasible, so analysis usually must be based on simplifications such as one-dimensional approximations of Earth structure.

A simple way to reduce the bias caused by focusing and defocusing is to use as data the ratios of amplitudes of seismic phases that follow similar paths, such as *P*:*SV*, *P*:*SH*, or *SH*:*SV*. If the ratio of the speeds of the waves involved is constant in the Earth, which usually is a good approximation, then in the geometrical-optics limit such amplitude ratios are unaffected by wave propagation. Amplitude ratios also have the advantage of being insensitive to instrument calibration.

Several workers have devised methods for using amplitude ratios to determine earthquake focal mechanisms. The algorithm of Pearce (1977, 1980) determines mechanisms constrained to be double couples from the ratios of amplitudes of teleseismic *P* and surface-reflected (*pP* or *sP*) phases, but because these have different ray paths in the source region, the ratios are still affected by structural heterogeneity there. Kisslinger *et al.* (1981) presented a method for local earthquakes, which uses ratios of the amplitudes of *P* and *SV* phases, both measured on commonly available vertical-component seismograms. Kisslinger's method also constrains the mechanisms to be double couples.

Both of these methods determine focal mechanisms by systematically searching through multi-dimensional parameter spaces. For double-couple mechanisms, the parameter space has three dimensions, and for general moment-tensor mechanisms, it has five. Computationally expensive searching methods are required because theoretical amplitudes and

amplitude ratios are strongly nonlinear functions of the fault parameters. Methods that use linearized approximations to iteratively perturb an initial estimate of the solution, which are often used in nonlinear inverse problems, perform poorly here because they find only locally optimum solutions and cannot detect multiple solutions, which commonly exist and may be radically different.

Nonlinearity and nonuniqueness are not inherent to the focal-mechanism problem, however, but are by-products of the double-couple source constraint. In terms of the moment-tensor source representation, the relation between source parameters and theoretical wave amplitudes is linear, and inversion methods based on this property are now common (for example, Stump and Johnson, 1977; Dziewonski *et al.,* 1981; Sipkin, 1987). As with any strictly linear inverse problem, conventional least-squares methods always produce a single solution.

Using certain types of data, such as polarities, also introduces nonlinearity into inverse problems. This is the reason, for example, that searching methods are still needed in an extension of the algorithm of Pearce (1977, 1980), which eliminates the *a priori* double-couple assumption and allows general moment-tensor sources (Pearce and Rogers, 1989). Nonlinear problems of this kind can be solved efficiently by applying linear-programming methods, which can treat inequalities, to the moment-tensor representation (Julian, 1978, 1986; Fitch *et al.,* 1980). Linear programming methods can also invert amplitude data expressed in terms of inequality constraints (Julian, 1986), can invert combined polarity and amplitude data robustly using the L1 norm (sum of the absolute values) of the residuals as a measure of goodness of fit (Fitch *et al.,* 1980), and can invert amplitudes of waves that have unknown polarities (Julian, 1986). Linear-programming problems cannot have distinct locally optimal solutions. The set of moment tensors consistent with a set of polarity and/or amplitude data is connected and convex, so any weighted average of consistent solutions is itself a consistent solution. Linear-programming methods can efficiently delineate this solution set by finding those members that are extreme in terms of physically motivated linear objective functions.

In this article, we extend the linear-programming inversion method of Julian (1978, 1986) to treat amplitude-ratio data. This extension is simple; an amplitude ratio turns out to be equivalent to a polarity, but with a modified Green's function. The extended method can invert any combination of polarity, amplitude, and amplitude-ratio data and is much more efficient than multi-dimensional searching.

Method

Polarities and Amplitudes

Arrange the six independent components of the 3×3 symmetric moment tensor in a column vector, $\mathbf{m}$. The amplitude of a seismic wave excited by a point source with moment tensor $\mathbf{m}$ can then be expressed as the dot product

$$u = \mathbf{g}^T\mathbf{m}, \tag{1}$$

where $\mathbf{g}$ is a column six-vector of Green's functions for the particular wave type and source and observer locations, and the superscript symbol T indicates transposition. The components of $\mathbf{g}$ corresponding to *P*, *SV*, and *SH* body waves in an infinite homogeneous isotropic elastic medium are given by Julian (1986). In the linear-programming method, observations are expressed as inequalities. For example, a polarity observation is expressed as either

$$\mathbf{g}^T\mathbf{m} \leqq 0 \text{ or } \mathbf{g}^T\mathbf{m} \geqq 0, \tag{2}$$

and an amplitude observation is expressed as the pair of inequalities,

$$\mathbf{g}^T\mathbf{m} \leqq a_{\max} \text{ and } \mathbf{g}^T\mathbf{m} \geqq a_{\max}, \tag{3}$$

for appropriate choices of the bounding values $a_{\max}$ and $a_{\min}$. By reversing the signs of amplitude bounds and Green's functions, we can express all these types of inequalities in the general form

$$\mathbf{g}^T\mathbf{m} \leqq a. \tag{4}$$

We wish to find a vector $\mathbf{m}$ consistent with a system of linear inequalities of the form (4). This is a linear-programming problem.

Amplitude Ratios

The approach described above is easily extended to handle amplitude ratios, by expressing each one as a pair of inequalities involving bounding values $r_{\min}$ and $r_{\max}$:

$$u^{(1)} \leqq r_{\max}u^{(2)}; \quad u^{(1)} \geqq r_{\min}u^{(2)}. \tag{5}$$

In terms of the Green's functions $\mathbf{g}^{(1)}$ and $\mathbf{g}^{(2)}$ for the two wave types involved, these inequalities are

$$\mathbf{g}^{(1)T}\mathbf{m} \leqq r_{\max}\mathbf{g}^{(2)T}\mathbf{m} \text{ and } \mathbf{g}^{(1)T}\mathbf{m} \geqq r_{\min}\mathbf{g}^{(2)T}\mathbf{m}. \tag{6}$$

Inequalities of this form apply only to amplitudes of known sign (i.e., to waves of known polarity); the formulation for unsigned (absolute value) amplitude observations is given in the Appendix. The pair of inequalities (6) can be written as

$$(\mathbf{g}^{(1)T} - r_{\max}\mathbf{g}^{(2)T})\,\mathbf{m} \leqq 0 \text{ and } (\mathbf{g}^{(1)T} - r_{\min}\mathbf{g}^{(2)T})\mathbf{m} \geqq 0, \tag{7}$$

which are in the same form as inequalities (2) for a pair of polarity observations but with different Green's functions. Inverting observed amplitude ratios is thus the same as inverting polarities, but with modified Green's functions.

Once the polarities and amplitude ratios are expressed as a system of inequality constraints of the form (4), we use the simplex algorithm (e.g., Dantzig, 1963) to seek a "feasible" solution, that is, a mechanism consistent with the constraints (Julian, 1986). The simplex algorithm does this by minimizing the "objective function"

$$F \stackrel{\text{def}}{=} \sum_{i \in S} |\mathbf{g}_i^T \mathbf{m} - a_i|, \tag{8}$$

where the subscript i is an index into the system of inequalities of the form (4) and S is the set of inequalities that are not satisfied. In terms of amplitudes, the objective function is the L1 norm of the residuals:

$$F = \sum_{i \in P} |u_i| + \sum_{i \in Q} |u_i - a_i| + \sum_{i \in R} |u_i^{(1)} - r_i u_i^{(2)}|, \tag{9}$$

where P is the set of polarity constraints that are not satisfied, Q is the set of amplitude constraints that are not satisfied, and R is the set of amplitude-ratio constraints that are not satisfied. The values a_i and r_i may be either the maximum or the minimum bounds from equations (3) and (6), depending on which bound is exceeded for each observation. Because the data are seldom of equal quality, we generalize F by applying a weight w_i to each observation:

$$F = \sum_{i \in P} w_i |u_i| + \sum_{i \in Q} w_i |u_i - a_i| + \sum_{i \in R} w_i |u_i^{(1)} - r_i u_i^{(2)}|. \tag{10}$$

If the minimum value for F found by the simplex algorithm is zero, then all the constraints are satisfied, and there is a nonempty set of feasible solutions. The simplex algorithm can then be applied again to maximize or minimize linear "objective" functions, for example, to identify superfluous constraints or to delimit the solution set by finding those feasible mechanisms that are extreme in terms of physical quantities such as volume change.

Graphical Representation of Amplitude Ratios

In graphical displays, we represent an amplitude ratio A:B by an arrow of unit length, oriented so that its slope equals A/B (Fig. 1). The signs of A and B are taken into account so that the arrow points to the right or left accordingly as B is positive or negative, and up or down accordingly as A is positive or negative. The orientation of an arrow is independent of its position on the focal sphere. This display method should not be confused with that commonly used to represent a particle-motion direction. Its advantage over methods that use symbols of different sizes is that it does not place disproportionate emphasis on ratios with small denominators or small numerators.

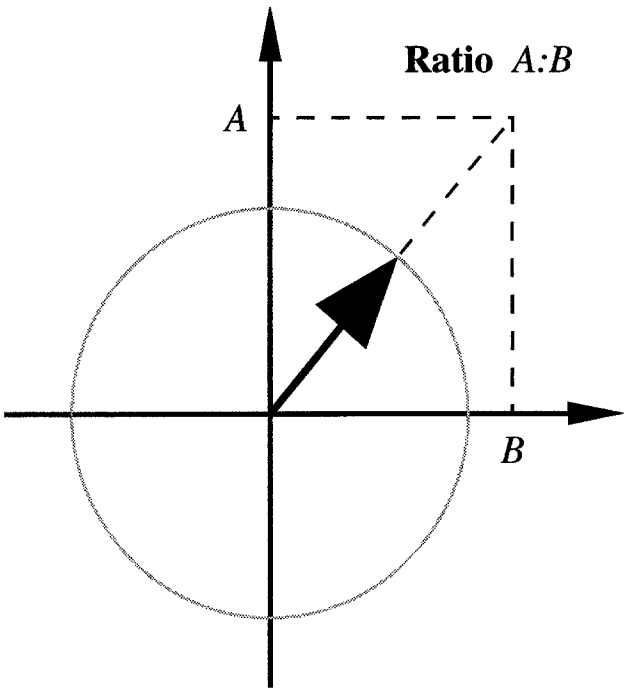

Figure 1. Graphical representation of amplitude ratios. The ratio A:B is represented by an arrow of unit length whose slope is A/B. Each quadrant corresponds to a unique combination of the signs of A and B. This representation has the advantages of (a) including information about the signs of the amplitudes A and B and (b) not causing strong visual distortion when one of the amplitudes is small.

Example

To illustrate the use of linear programming to invert amplitude ratios, we analyze an earthquake from the Hengill-Grensdalur geothermal area in southwestern Iceland. A geothermal area probably provides a rather severe test of the assumptions underlying the amplitude-ratio method, because geothermal fluids can cause large anomalies in the ratio V_P/V_S of the seismic-wave speeds (Julian *et al.*, 1996b). The Hengill-Grensdalur area is known, on the basis of first-motion studies, to be a rich source of non-double-couple earthquakes (Foulger and Long, 1984; Foulger, 1988; Foulger and Julian, 1993; Julian *et al.*, 1996c), with mostly compressional P-wave polarities. During the summer of 1991, a network of 30 three-component seismometers, with natural frequencies of 2 Hz (Mark Products model L22D), were operated in an array about 25 km in diameter. The array geometry was designed, by tracing rays through a three-dimensional crustal model obtained in earlier work (Toomey and Foulger, 1989), to provide approximately uniform focal-sphere coverage for earthquakes in the area of greatest activity. About 4000 earthquakes were recorded digitally on REFTEK model 72A-02 Data Acquisition Systems at a rate of 100 samples/sec.

Table 1 gives the hypocentral coordinates of the earthquake and the measured wave amplitudes. P waves were

Table 1
Observed Amplitudes for Earthquake of 15 September 1991, 07:41:28 UTC, 64.0309° N, 21.2144° W, Depth 3.94 km Moment Magnitude 1.7

Station	Δ* (km)	ϕ† (°)	θ‡ (°)	P§	Amplitude SH¶ (Counts)	SV‖
H001	13.69	225	93	−2.05		
H004	12.62	259	94	−3.67	9.00	
H005	3.59	210	129	4.62	−20.43	
H006	6.84	122	104	4.07	26.56	
H007	1.77	143	151	5.82	−26.82	33.30
H008	7.73	88	101	−4.17		
H009	3.44	64	131	−1.74	−5.03	24.02
H010	0.08	332	179	34.81	−116.5	−236.6
H011	2.05	290	148	29.86	114.7	75.92
H012	2.46	22	142	35.59	−163.4	
H014	4.02	352	125	89.46	−165.7	
H015	3.47	312	130	30.81	114.3	
H016	5.05	267	116		105.0	
H017	7.45	272	102	−2.43	72.94	
H018	2.06	338	147	56.61	−54.54	125.9
H021	10.55	317	95	12.40	33.24	
H024	5.15	2	115	56.71	−80.34	
H025	5.23	25	114	12.96	−90.07	
H026	8.15	50	100	−3.00	−48.47	
H028	10.91	1	95	11.47		
H029	9.91	333	96	8.30		
H031	18.81	342	74	2.78		
H033	5.63	296	112	9.02	74.46	
H034	6.42	341	107	20.62		
H035	11.43	31	95	0.77	−8.52	
H036	11.11	152	95	7.39	14.11	

*Epicentral distance.
†Azimuth of departing ray, measured clockwise from north.
‡Take-off angle, measured from nadir.
§Positive for outward motion.
¶Positive for clockwise motion about the epicenter.
‖Positive for motion toward the epicenter.

measured on vertical-component seismograms and *SH* and *SV* waves were measured on transverse- and radial-component seismograms numerically rotated from the field orientations. To minimize distortion from wave-propagation effects such as scattering and anelastic attenuation, we first low-pass filtered the seismograms, using a three-pole Butterworth digital filter with a corner frequency of 5 Hz, chosen by visual inspection of the outputs from various filters. Amplitudes were measured from the onset to the first peak, and only signals with similar rise times were used in ratios. Figure 2 shows raw and filtered seismograms for two stations and illustrates how the amplitudes were measured.

We mapped observations onto the focal sphere by numerically tracing rays (Julian and Gubbins, 1977) through the three-dimensional tomographic model of Foulger *et al.* (1995). Before inverting amplitude ratios, we corrected the amplitudes for mode conversion at the free surface, assuming plane waves incident at the surface of a homogeneous half-space with $V_P/V_S = 1.78$ (Foulger *et al.*, 1995). To avoid complicated mode-conversion effects, we used *SV* waves only if they emerged at the surface within 25° of the vertical direction. We corrected for wave attenuation (which affects compressional and shear waves differently and thus alters *P*:*S* amplitude ratios) using crustal Q_P and Q_S values measured in southwestern Iceland by Menke *et al.* (1995). We also multiplied each amplitude by the cube of the wave speed at the focus, to compensate for the systematic difference between the radiated amplitudes of compressional and shear waves (see, for example, equations 4.91 of Aki and Richards, 1980).

Polarity observations alone (the signs of the amplitudes in Table 1) do not constrain the mechanism well, even though the data are unusually well distributed on the focal sphere. Figure 3 shows the observed *P*, *SH*, and *SV* polarities and compares them with the theoretical nodal surfaces for three mechanisms, whose moment tensors are given in Table 2. The first two mechanisms, obtained by linear programming analysis, are consistent with all the observed first motions. The "EXPLOSIVE" mechanism maximizes the trace of the moment tensor and the "IMPLOSIVE" mechanism minimizes it. The "DOUBLE COUPLE" mechanism is the major double-couple component of the IMPLOSIVE mechanism. Because we invert only polarities and no amplitudes, the components of each moment tensor are undetermined within an arbitrary factor, and the values in Table 2 are therefore normalized arbitrarily. Table 2 also gives the relative moments of the volumetric, double-couple, and "compensated linear-vector dipole" (CLVD) components (Julian *et al.*, 1996a) of each solution. Mechanisms consistent with the data range from dominantly explosive to nearly deviatoric, and strictly deviatoric mechanisms such as the double couple shown provide acceptable, though not perfect, fits. Furthermore, *S*-wave polarities provide little additional constraint. All the solutions consistent with the *P*-wave polarities predict nearly identical *SH*- and *SV*-wave polarity distributions.

The observed amplitude ratios, on the other hand, rule out double-couple interpretations and require the mechanism to have a large explosive isotropic component. Figure 4 compares the observed *P*:*SH* and *SH*:*SV* amplitude ratios with the theoretical ratios for both the double-couple solution of Figure 3 and the mechanism obtained by inverting polarities and amplitude ratios simultaneously. Clearly, the inversion-derived mechanism fits the data much better than the double couple. Figure 5 compares the observed polarities with the theoretical polarity fields for this mechanism, which is similar to the EXPLOSIVE mechanism shown in Figure 3.

The need for an isotropic component can be understood intuitively. The focal-sphere coverage is good, and any double-couple mechanism consistent with the polarities must resemble closely the one shown. Several of the observed *P* arrivals lie close to nodal planes of this mechanism and thus should have small amplitudes and appear as nearly horizontal arrows on Figure 4. On the contrary, the observed amplitudes of these *P* waves are roughly comparable to the *SH* amplitudes and, thus, are inconsistent with a double-couple interpretation.

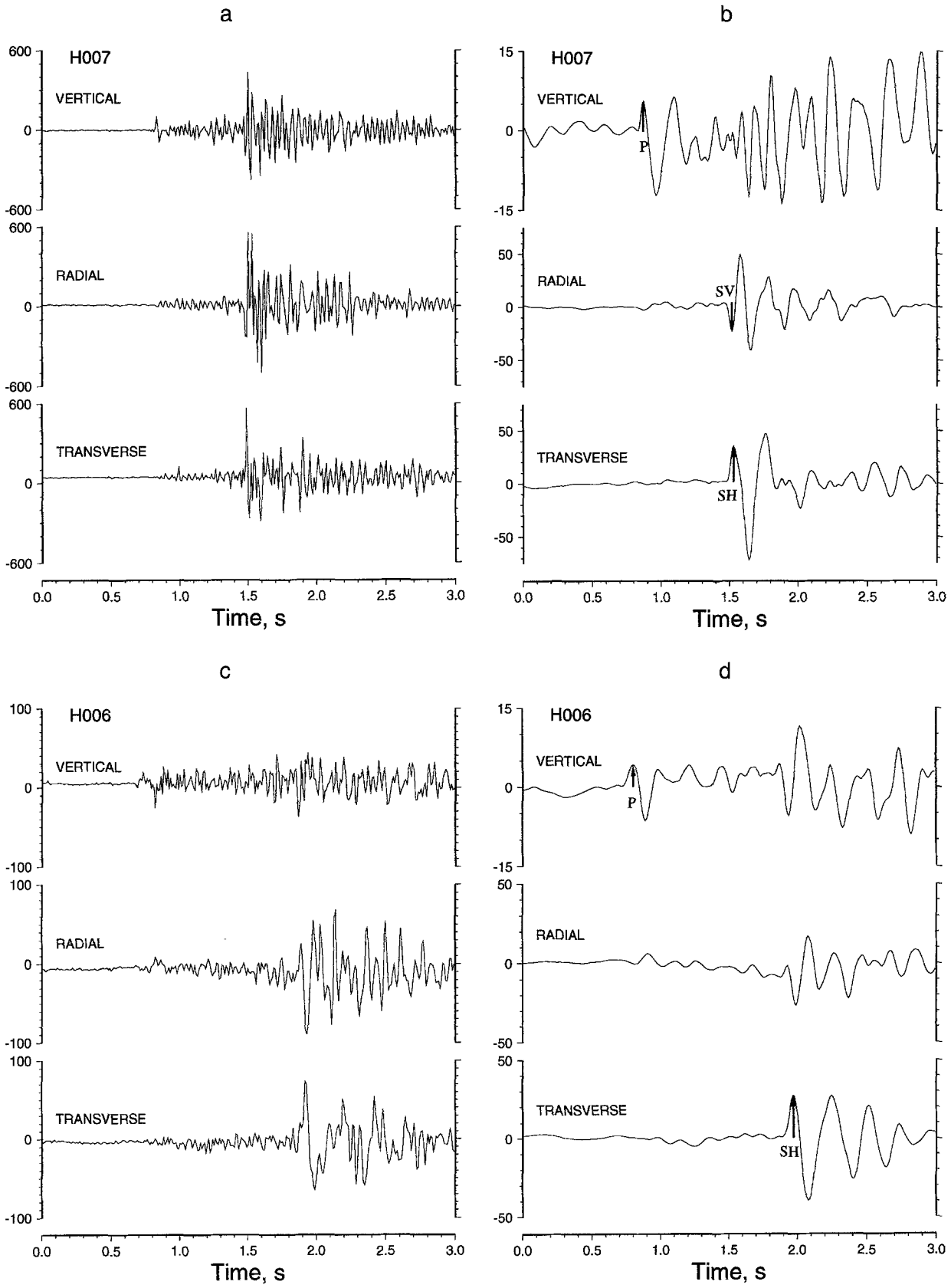

Figure 2. Rotated seismograms for earthquake of 07:41 UTC, 15 September 1991 at the Hengill geothermal area, Iceland, considered in the example. (a) Station H007. (b) Station H007, filtered. (c) Station H006. (d) Station H006, filtered. Ordinate: digital counts (1 count = 3.2×10^{-10} m). Filter has three-pole Butterworth low-pass response, with corner frequency 5 Hz. Arrows indicate amplitudes given in Table 1 and used in inversion. Note large signal/noise ratio on transverse components.

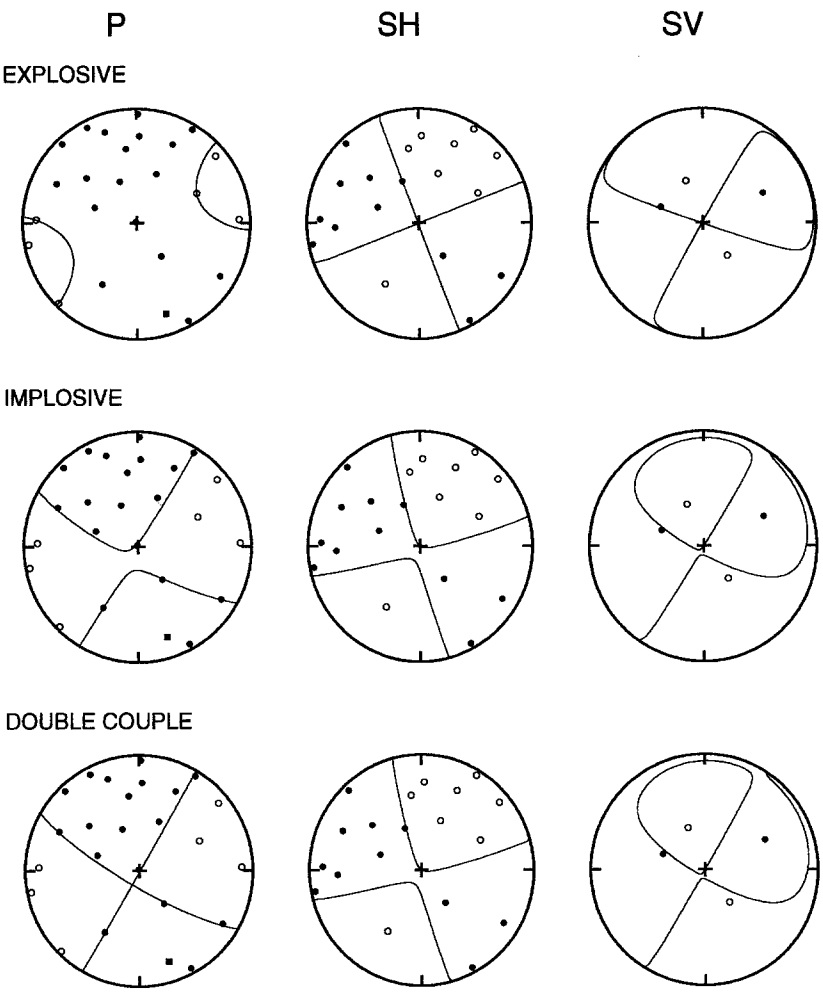

Figure 3. Three different focal mechanisms that are consistent or nearly consistent with *P*- and *S*-wave polarities for the earthquake of 15 September 1991 07:41 UTC at the Hengill geothermal area, Iceland. The "EXPLOSIVE" mechanism maximizes the trace of the moment tensor, and the "IMPLOSIVE" mechanism minimizes it. The "DOUBLE COUPLE" mechanism is the principal double-couple component of the IMPLOSIVE mechanism. Even with well-distributed stations, first-motion polarities can seldom resolve focal mechanisms well if general (moment-tensor) point sources are allowed. Including *SH* and *SV* polarity data does not help to identify the correct mechanism in this case. Upper focal hemispheres are shown in equal-area projection. Black symbols indicate positive polarities, and open symbols indicate negative polarities. Squares represent lower-hemisphere values plotted at their antinodal points.

Table 2
Derived Focal Mechanisms

	M_{xx}	M_{xy}	M_{yy}	M_{xz}	M_{yz}	M_{zz}	Vol.	DC	CLVD
EXPLOSIVE	5.303	−2.512	−0.303	0.0	0.094	1.789	36%	49%	15%
IMPLOSIVE	3.568	−1.978	−3.325	−0.445	0.634	−0.050	2%	92%	6%
DC	8.504	−4.879	−8.533	−1.017	1.610	0.029	0%	100%	0%
BEST	4.277	−1.661	−1.049	0.417	0.286	2.309	35%	47%	18%

x axis directed north, y axis directed east, z axis directed down.

Amplitude Ratios Versus Amplitudes

We also inverted amplitudes (rather than ratios) directly, to test the assumption that amplitude ratios are less seriously distorted than amplitudes by propagation effects and to determine how well this distortion might be corrected. We corrected the observed amplitudes for mode conversion at the surface and wave attenuation, as described above. We also corrected for geometric spreading, which is available as a by-product of the three-dimensional numerical raytracing computations.

In evaluating different solutions, we use as a measure of goodness of fit the mean absolute relative deviation (MARD), defined for amplitudes as

$$E \overset{\text{def}}{=} \frac{1}{N}\sum_{i=1}^{N}\left|\frac{u_i - a_i}{a_i}\right| \tag{11}$$

and for amplitude ratios as

$$E \overset{\text{def}}{=} \frac{1}{N}\sum_{i=1}^{N}\left|\frac{a_i^{(2)}u_i^{(1)} - a_i^{(1)}u_i^{(2)}}{a_i^{(1)}u_i^{(1)} + a_i^{(2)}u_i^{(2)}}\right| \tag{12}$$

In these equations, a_i, $a_i^{(1)}$, and $a_i^{(2)}$ are observed amplitudes and u_i, $u_i^{(1)}$, and $u_i^{(2)}$ are the corresponding theoretical am-

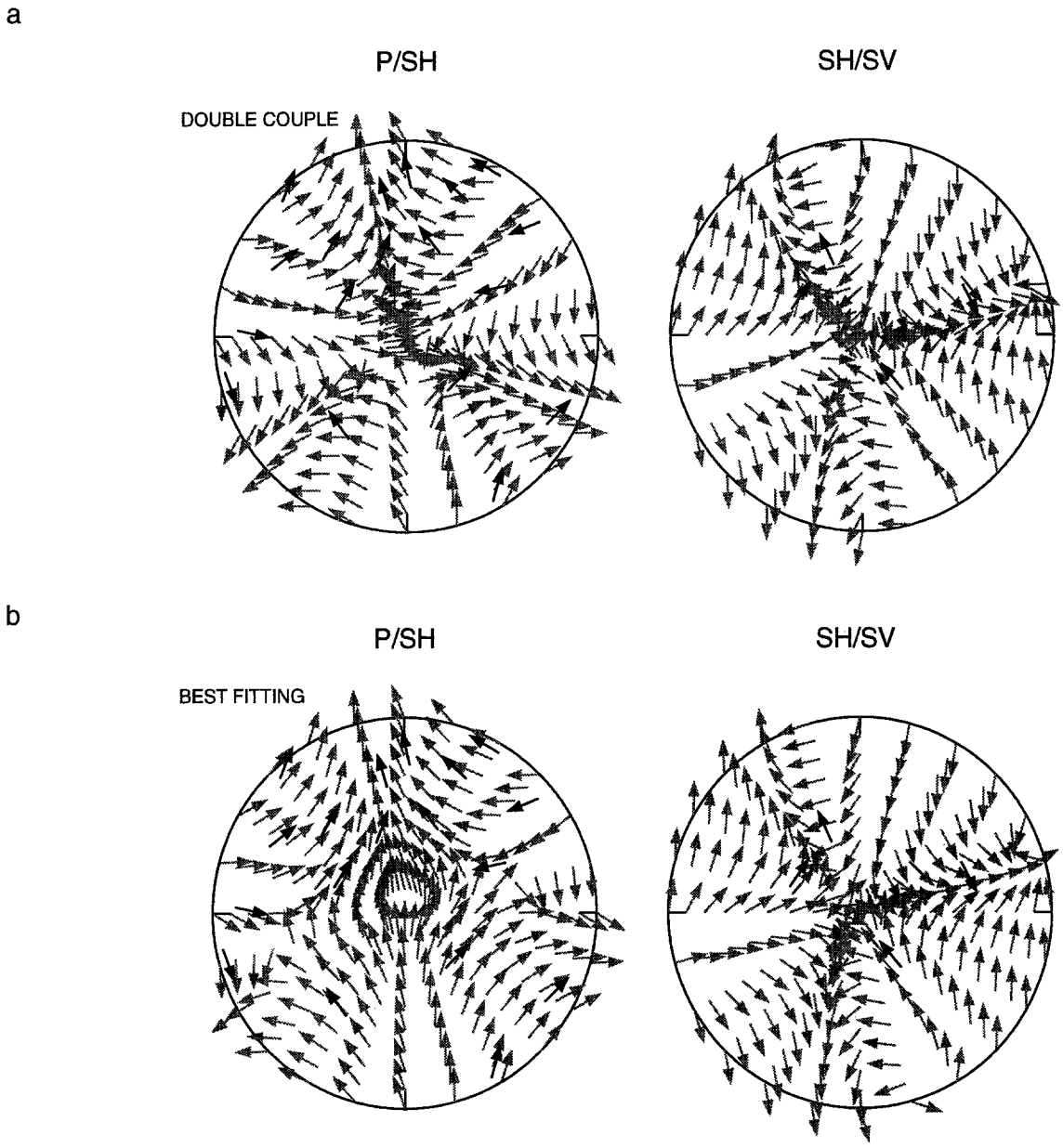

Figure 4. (a) Comparison of observed *P*:*SH* and *SH*:*SV* amplitude ratios (black arrows) with theoretical ratios (gray arrows) for the double-couple mechanism shown in Figure 3. *P*:*SH* ratios are multiplied by the quantity $(V_P/V_S)^3$. (b) Same as (a), for the mechanism obtained by simultaneously inverting polarity and amplitude-ratio data using the linear-programming method. This mechanism fits the data much better than the double couple and is similar to the EXPLOSIVE mechanism shown in Figure 3. Amplitude ratios are represented as arrows (see Fig. 1) and are plotted on equal-area projections of upper focal hemispheres.

plitudes. The quantity whose absolute value appears on the right-hand side of equation (12) is the tangent of the angle between the vectors representing an observed and a theoretical ratio, in the graphical representation shown in Figure 1.

We can choose the constants w_i and r_i in equation (10) so that for amplitudes the objective function F is identical (except for a constant factor N) to the MARD E given in equation (11) and the simplex algorithm minimizes E. It is not possible, however, to establish such a correspondence for amplitude ratios, because the denominator in equation (12) contains the unknown quantities $u_i^{(1)}$ and $u_i^{(2)}$. Therefore, in amplitude-ratio inversion, we must use a suboptimal objective function, and the MARD obtained is not optimal.

Nevertheless, we obtain a significantly better fit to amplitude ratios than to amplitudes. For amplitude ratios, the MARD obtained (with no geometric-spreading correction) is

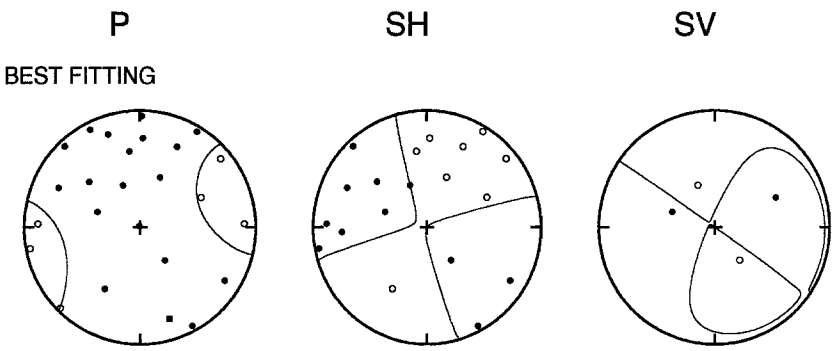

Figure 5. Comparison of polarity data with nodal surfaces for the best-fitting focal mechanism of Figure 4(b). Plotting conventions as in Figure 3.

0.294, whereas for amplitudes, it is 0.426 when spreading corrections are applied and 0.678 when they are not. These results support the basic assumption on which this article is based: that wave propagation distorts amplitudes more than it does amplitude ratios.

Conclusions

Wave polarities, even when they include multiple seismic phases and cover the focal sphere well, provide poor resolution of earthquake focal mechanisms, if general moment-tensor sources are allowed. To resolve mechanisms well, other types of observations, such as wave amplitudes, must be used, but amplitudes are severely distorted by wave propagation in the Earth.

The ratios of the amplitudes of appropriately chosen seismic phases are comparatively insensitive to distortion by structural complexity and thus provide better constraints on the focal mechanisms of earthquakes than do simple amplitudes. Amplitude ratios can be inverted using a simple extension of the linear-programming method (Julian, 1986), which is far more efficient than multi-parameter searching, especially when the solutions are free from artificial (e.g., double-couple) constraints.

Amplitude ratios from an earthquake at the Hengill-Grensdalur geothermal area in southwestern Iceland can be fitted within a mean absolute relative deviation of 0.294, while amplitudes can be fitted only to within about 0.426. For this earthquake, amplitude ratios (primarily *P*:*SH*) require a large volumetric component, which even unusually well-distributed multi-phase (*P*, *SH*, *SV*) polarity data cannot resolve.

Appendix

Absolute Amplitude Ratios

The inversion method presented in the text deals with ratios of signed amplitudes, that is, with waves whose polarities are known. It often happens, however, that amplitudes can be determined reliably even when polarities cannot. In this appendix, we show how to invert ratios of unsigned amplitudes, thereby extending the inversion method to waves with unknown polarities. The method is similar to the one given by Julian (1986) for inverting absolute amplitudes.

Consider a pair of inequality constraints similar to those in equation (6), but involving absolute values of amplitudes,

$$C^{(1)}|\mathbf{g}^{(1)T}\mathbf{m}| \geqq C^{(2)}\,|\mathbf{g}^{(2)T}\mathbf{m}|, \tag{A1}$$

and

$$D^{(1)}|\mathbf{g}^{(1)T}\mathbf{m}| \leqq D^{(2)}|\mathbf{g}^{(2)T}\mathbf{m}|. \tag{A2}$$

Introduce non-negative auxiliary "slack" and "error" variables $s^{(1)}$, $e^{(1)}$, $s^{(2)}$, and $e^{(2)}$, defined by

$$\mathbf{g}^{(1)T}\mathbf{m} + s^{(1)} - e^{(1)} = 0 \tag{A3}$$

and

$$\mathbf{g}^{(2)T}\mathbf{m} + s^{(2)} - e^{(2)} = 0, \tag{A4}$$

with the additional constraints

$$s^{(1)} = 0 \text{ or } e^{(1)} = 0 \tag{A5}$$

and

$$s^{(2)} = 0 \text{ or } e^{(2)} = 0. \tag{A6}$$

Because of these constraints, the absolute value of each amplitude is equal to the sum of its slack and error variables,

$$|\mathbf{g}^{(1)T}\mathbf{m}| = s^{(1)} + e^{(1)} \text{ and } |\mathbf{g}^{(2)T}\mathbf{m}| = s^{(2)} + e^{(2)}, \tag{A7}$$

so the inequality constraints (A1) and (A2) can be expressed as the pair of equations

$$C^{(1)}(s^{(1)} + e^{(1)}) - C^{(2)}(s^{(2)} + e^{(2)}) - x = 0 \tag{A8}$$

and

$$D^{(1)}(s^{(1)} + e^{(1)}) - D^{(2)}(s^{(2)} + e^{(2)}) + y = 0 \tag{A9}$$

involving two more auxiliary variables, x and y (again non-

negative with one of them equal to zero). Thus, the pair of inequality constraints on absolute amplitude ratios (A1) and (A2) adds four equations, (A3), (A4), (A8), and (A9), to the linear programming problem and introduces six auxiliary variables.

Acknowledgments

Paul Spudich and Jon Fletcher reviewed the manuscript, and their suggestions led to substantial improvements. The data used in the example were collected using instruments lent by the IRIS/PASSCAL and NERC instrument pools, in a project supported by a G. K. Gilbert Fellowship from the U.S. Geological Survey and NERC Grant GR9/134. Any use of trade, firm, or product names and trademarks in this publication is for descriptive purposes only and does not constitute endorsement by the U.S. Government.

References

Aki, K. and P. G. Richards (1980). *Quantitative Seismology,* Vol. I, Freeman, New York, 557 pp.

Dantzig, G. B. (1963). *Linear Programming and Extensions,* Princeton University Press, Princeton, 627 pp.

Dziewonski, A. M., T.-A. Chou, and J. G. Woodhouse (1981). Determination of earthquake source parameters from wave-form data for studies of global and regional seismicity, *J. Geophys. Res.* **86,** 2825–2852.

Fitch, T. J., D. W. McCowan, and M. W. Shields (1980). Estimation of the seismic moment tensor from teleseismic body wave data with applications to intraplate and mantle earthquakes, *J. Geophys. Res.* **85,** 3817–3828.

Foulger, G. R. and R. E. Long (1984). Anomalous focal mechanism solutions: evidence for tensile crack formation on an accreting plate boundary, *Nature* **310,** 43–45.

Foulger, G. R. (1988). The Hengill triple junction, SW Iceland: 2. Anomalous earthquake focal mechanisms and implications for process within the geothermal reservoir and at accretionary plate boundaries, *J. Geophys. Res.* **93,** 13507–13523.

Foulger, G. R. and B. R. Julian (1993). Non-double-couple earthquakes at the Hengill-Grensdalur volcanic complex, Iceland: Are they artifacts of crustal heterogeneity?, *Bull. Seism. Soc. Am.* **83,** 38–52.

Foulger, G. R., A. D. Miller, B. R. Julian, and J. R. Evans (1995). Three-dimensional v_P and v_P/v_S structures of the Hengill triple junction and geothermal area, Iceland and the repeatability of tomographic inversions, *Geophys. Res. Lett.* **22,** 1309–1312.

Julian, B. R. (1978). An inverse method for earthquake source mechanisms, *Tectonophysics* **49,** 223.

Julian, B. R. (1986). Analysing seismic-source mechanisms by linear-programming methods, *Geophys. J. R. Astr. Soc.* **84,** 431–443.

Julian, B. R. and D. Gubbins (1977). Three-dimensional seismic ray tracing, *J. Geophys.* **43,** 95–113.

Julian, B. R., A. D. Miller, and G. R. Foulger (1996a). Non-double-couple earthquakes I. Theory, *Rev. Geophys.,* accepted.

Julian, B. R., A. Ross, G. R. Foulger, and J. R. Evans (1996b). Three-dimensional seismic image of a geothermal reservoir: the Geysers, California, *Geophys. Res. Lett.,* **23,** 685–688.

Julian, B. R., A. D. Miller, and G. R. Foulger (1996c). Non-double-couple earthquake mechanisms at the Hengill-Grensdalur volcanic complex, southwest Iceland, *Geophys. Res. Lett.*, in press.

Kisslinger, C., J. R. Bowman, and L. Koch (1981). Procedures for computing focal mechanisms from local (*SV/P*) data, *Bull. Seism. Soc. Am.* **71,** 1719–1729.

Menke, W., V. Levin, and R. Sethi (1995). Seismic attenuation in the crust at the mid-Atlantic plate boundary in south-west Iceland, *Geophys. J. Int.* **122,** 175–182.

Miller, A. D., G. R. Foulger, and B. R. Julian (1996). Non-double-couple earthquakes II. Observations, *Rev. Geophys.,* submitted.

Pearce, R. G. (1977). Fault plane solutions using relative amplitudes of *P* and *pP*, *Geophys. J. R. Astr. Soc.* **50,** 381–394.

Pearce, R. G. (1980). Fault plane solutions using relative amplitudes of *P* and surface reflections: further studies, *Geophys. J. R. Astr. Soc.* **60,** 459–487.

Pearce, R. G. and R. M. Rogers (1989). Determination of earthquake moment tensors from teleseismic relative amplitude observations, *J. Geophys. Res.* **94,** 775–786.

Sipkin, S. A. (1987). Moment tensor solutions estimated using optimal filter theory, *Phys. Earth Planet. Interiors* **47,** 67–79.

Stump, B. W. and L. R. Johnson (1977). The determination of source properties by the linear inversion of seismograms, *Bull. Seism. Soc. Am.* **67,** 1489–1502.

Toomey, D. R. and G. R. Foulger (1989). Application of tomographic inversion to local earthquake data from the Hengill-Grensdalur central volcano complex, Iceland, *J. Geophys. Res.* **94,** 17497–17510.

U.S. Geological Survey
345 Middlefield Rd. MS977
Menlo Park, California 94025
(B. R. J.)

Department of Geological Sciences
University of Durham
Durham DH1 3LE, U.K.
(G. R. F.)

Manuscript received 23 May 1994.